

Stochastic Trajectories and Spectral Boundary Conditions for Enhanced Diffusion in Immersed Boundary Problems

Rômulo Damasclin Chaves dos Santos
Technological Institute of Aeronautics
romulosantos@ita.br

Jorge Henrique de Oliveira Sales
Santa Cruz State University
jhosales@uesc.br

October 31, 2024

Abstract

This work presents a comprehensive framework for enhanced diffusion modeling in fluid-structure interactions by combining the Immersed Boundary Method (IBM) with stochastic trajectories and high-order spectral boundary conditions. Using semi-Lagrangian schemes, this approach captures complex diffusion dynamics at moving interfaces, integrating probabilistic methods that reflect multi-scale fluctuations. In addition to a rigorous mathematical foundation that includes stability proofs, this model exhibits reduced numerical diffusion errors and improved stability in long-term simulations. Comparative studies highlight its effectiveness in multi-scale scenarios that require precision in interface dynamics. Focusing on various shear and circular flows, including those with Hölder and Lipschitz regularities and critical points, we establish sharp bounds on effective diffusion rates using specific initial data examples. This dual exploration in enhanced diffusion highlights how flow regularity and critical points influence dissipation. These findings advance both the theoretical understanding and practical applications of enhanced diffusion in fluid dynamics, offering new insights into diffusion rate optimization through interface dynamics and flow structure regularities. Future research can

further refine the IBM framework by exploring alternative probabilistic methods to improve interface accuracy, opening up the potential for improved modeling in applications that require precise control over mixing rates and dissipation processes.

Keywords: Stochastic Trajectories. Advection-Diffusion Equation. Dissipation Estimation. Feynman-Kac Theorem.

Contents

1	Introduction	3
2	The Mathematical Theory	3
3	Proof of Enhanced Dissipation via Stochastic Trajectories	5
3.1	Definition of Stochastic Trajectories	5
3.2	Calculation of Energy Dissipation	5
3.3	Estimate of Dissipation via Variance	6
3.3.1	Feynman-Kac Relation	6
3.3.2	Variance and Dissipation	6
3.3.3	Applying Itô's Formula and Jensen's Inequality	7
3.3.4	Relation to Spatial Integral	7
3.3.5	Derivation of the Formulation	7
4	Regular Shear Flows with Critical Points	9
5	Hölder and Lipschitz Shear Flows	9
6	Circular Flows	9
7	Anisotropic Enhanced Diffusion in Circular Flows Theorem	10
7.1	Proof of the Theorem	10
7.1.1	Governing Equation	11
7.1.2	Initial Condition Setup	11
7.1.3	Scaling Analysis of the Diffusion Term	11
7.1.4	Characterizing the Mixing Dynamics	12
7.1.5	Asymptotic Behavior as $\kappa \rightarrow 0$	12
7.1.6	Balancing Radial and Angular Contributions	12
7.1.7	Complete Expression for Mixing Time	12
8	Results	13

1 Introduction

The study of enhanced diffusion in fluid-structure interactions has been a significant area of mathematical and computational research. Early work in the 1990s, such as [1], established foundational principles for diffusion in passive advection. Advancements by Bedrossian and Zelati [2] introduced hypocoercivity in shear flows, which broadened our understanding of dissipation in complex flows. More recent studies by Coti Zelati et al. [3] introduced stochastic models to analyze dissipation at multiple time scales, further inspiring our current approach.

In parallel, the Immersed Boundary Method (IBM), initially proposed by Peskin [5], provided a numerical technique for handling interfaces within fluids, primarily in biological applications. The IBM has evolved to integrate spectral methods and adaptive mesh refinement [6], enhancing its ability to model fine-scale dynamics in fluid-structure interactions.

Building on these advances, the present approach proposes a hybrid framework that applies stochastic trajectories together with IBM to model dissipation. This model is particularly beneficial in contexts where interfaces are complex and traditional IBM approaches can suffer from significant numerical diffusion. Using high-order spectral conditions near the boundary, the model effectively minimizes errors in the region surrounding the interface. It is hypothesized that the combination of stochastic trajectories and semi-Lagrangian schemes will offer an improved framework for simulations that require both accuracy and computational efficiency.

2 The Mathematical Theory

Consider the advection-diffusion equation for a scalar quantity ρ subjected to an incompressible velocity field $\mathbf{u}(x, y)$:

$$\partial_t \rho + \mathbf{u} \cdot \nabla \rho = \kappa \Delta \rho, \quad (1)$$

where $\kappa > 0$ is a constant diffusivity that characterizes the rate of diffusion of the scalar quantity. This equation models the transport and spread of quantities such as pollutants, heat, or other scalars in a fluid medium.

To enhance the analysis of diffusion in this context, we introduce stochastic trajectories $X_{t,s}$, which can be interpreted as the paths traced by particles

in the fluid influenced by both the deterministic advection and random diffusion effects. Following the work of Coti-Zelati *et al.* [4], we describe these trajectories using a backward Itô process:

$$dX_{t,s} = \mathbf{u}(X_{t,s}) ds + \sqrt{2\kappa} dB_s, \quad (2)$$

where B_s denotes a standard Brownian motion. The term $\sqrt{2\kappa} dB_s$ introduces stochasticity, capturing the random diffusion component, while the advection term $\mathbf{u}(X_{t,s}) ds$ governs the deterministic motion according to the velocity field.

Using the Feynman-Kac formula, we express the solution to the advection-diffusion equation as an expected value along these stochastic paths:

$$\rho(t, x) = \mathbb{E}[\rho_0(X_{t,0}(x))], \quad (3)$$

where ρ_0 represents the initial condition of the scalar field. This formulation allows us to understand how initial conditions evolve over time as particles follow the stochastic trajectories.

To accurately capture the behavior near interfaces, we implement semi-Lagrangian Immersed Boundary Method (IBM) techniques. These techniques enable the treatment of complex geometries and interfaces within the computational domain. We use spectral boundary conditions to model the interaction of the scalar field with the interface Γ . This is represented mathematically as:

$$\rho_\Gamma = \int_\Gamma \delta_\epsilon(X - X_\Gamma) \rho dS, \quad (4)$$

where δ_ϵ is a regularized delta function that approximates the delta function near the interface. The regularization parameter ϵ controls the spread of the delta function, ensuring that it captures the contributions from the scalar field in a smooth manner while respecting the geometric complexities of the interface.

In summary, the combination of stochastic trajectories and semi-Lagrangian techniques enhances our ability to analyze the advection-diffusion process, particularly in complex domains where traditional methods may struggle. This approach provides a robust framework for studying the transport phenomena of scalar quantities influenced by both deterministic and stochastic processes.

3 Proof of Enhanced Dissipation via Stochastic Trajectories

Consider the advection-diffusion equation for a scalar quantity ρ , subject to an incompressible velocity field \mathbf{u} :

$$\partial_t \rho + \mathbf{u} \cdot \nabla \rho = \kappa \Delta \rho, \quad (5)$$

where $\kappa \in (0, 1)$ is a diffusion parameter. The goal is to demonstrate that the use of stochastic trajectories $X_{t,0}(x)$, described by a backward Itô process, provides an estimate for the energy dissipation that enhances the standard diffusion rate.

3.1 Definition of Stochastic Trajectories

We introduce stochastic trajectories $X_{t,s}$ that describe the behavior of a particle under the velocity field \mathbf{u} , with additive noise to capture the effects of diffusion:

$$dX_{t,s} = \mathbf{u}(X_{t,s}) ds + 2\kappa dB_s, \quad X_{t,t} = x, \quad (6)$$

where B_s is Brownian motion, and $X_{t,s}$ represents the position at time s of a particle that arrives at point x at time t . We use the Feynman-Kac formula to express the solution $\rho(t, x)$ along these trajectories, obtaining:

$$\rho(t, x) = \mathbb{E}[\rho_0(X_{t,0}(x))], \quad (7)$$

where ρ_0 is the initial condition.

3.2 Calculation of Energy Dissipation

To quantify the dissipation, we consider the decay rate of the L^2 norm of ρ over time. The total energy of ρ satisfies the following identity:

$$\frac{1}{2} \frac{d}{dt} \|\rho(t)\|_{L^2}^2 + \kappa \|\nabla \rho(t)\|_{L^2}^2 = 0. \quad (8)$$

Integrating with respect to time, we obtain:

$$\frac{1}{2} \|\rho(t)\|_{L^2}^2 + \kappa \int_0^t \|\nabla \rho(s)\|_{L^2}^2 ds = \frac{1}{2} \|\rho_0\|_{L^2}^2. \quad (9)$$

3.3 Estimate of Dissipation via Variance

To estimate the dissipation of energy in the context of the advection-diffusion equation, we invoke the Feynman-Kac theorem, which connects stochastic processes with partial differential equations. Specifically, we consider the advection-diffusion equation given by:

$$\partial_t \rho + u \cdot \nabla \rho = \kappa \Delta \rho, \quad (10)$$

where $\rho = \rho(t, x)$ represents the scalar quantity being diffused, u is the incompressible velocity field, and κ is the diffusivity coefficient.

3.3.1 Feynman-Kac Relation

By utilizing the Feynman-Kac theorem, we can express the solution $\rho(t, x)$ in terms of expected values along stochastic trajectories. The trajectories are defined by the stochastic differential equation:

$$dX_{t,s} = u(X_{t,s}) ds + \sqrt{2\kappa} dB_s, \quad (11)$$

where B_s is a standard Brownian motion. The solution to the advection-diffusion equation can then be expressed as:

$$\rho(t, x) = \mathbb{E}[\rho_0(X_{t,0}(x))], \quad (12)$$

where ρ_0 is the initial condition at time $t = 0$.

3.3.2 Variance and Dissipation

To quantify the dissipation of energy, we focus on the dissipation represented by the L^2 -norm of the gradient of ρ . We relate this to the variance of the initial condition sampled along the stochastic trajectories:

$$\kappa \int_0^t \|\nabla \rho(s)\|_{L^2}^2 ds = \frac{1}{2} \int_{\Omega} \text{Var}(\rho_0(X_{t,0}(x))) dx. \quad (13)$$

Here, the variance of $\rho_0(X_{t,0}(x))$ is defined as:

$$\text{Var}(\rho_0(X_{t,0}(x))) = \mathbb{E} [(\rho_0(X_{t,0}(x)) - \mathbb{E}[\rho_0(X_{t,0}(x))])^2]. \quad (14)$$

3.3.3 Applying Itô's Formula and Jensen's Inequality

Let $f(x) = \rho_0(X_{t,0}(x))$. To derive an upper estimate for the variance, we apply Itô's formula, which provides a way to compute the dynamics of $f(X_{t,s})$. Applying Itô's lemma gives us:

$$\begin{aligned} df(X_{t,s}) &= \nabla f \cdot dX_{t,s} + \frac{1}{2} \Delta f ds \\ &= \nabla f \cdot \left(u(X_{t,s}) ds + \sqrt{2\kappa} dB_s \right) + \frac{1}{2} \Delta f ds. \end{aligned}$$

Taking expectations and using the properties of Brownian motion, we can simplify and analyze the growth of f :

$$d\mathbb{E}[f(X_{t,s})] = \mathbb{E}[\nabla f \cdot u(X_{t,s}) ds] + \kappa \mathbb{E}[\Delta f] ds.$$

Consequently, we can apply Jensen's inequality to obtain an upper bound for the variance:

$$\begin{aligned} \text{Var}(\rho_0(X_{t,0}(x))) &\leq \mathbb{E}[\rho_0(X_{t,0}(x))^2] - \mathbb{E}[\rho_0(X_{t,0}(x))]^2 \\ &\leq \mathbb{E}[f(X_{t,0})^2] \leq (\mathbb{E}[f(X_{t,0})])^2 + \mathbb{E}[(\nabla f)^2], \end{aligned}$$

where ∇f denotes the spatial gradient of f .

3.3.4 Relation to Spatial Integral

Applying these results allows us to relate the variance to the integral over the spatial domain. Therefore, we have:

$$\kappa \int_0^t \|\nabla \rho(s)\|_{L^2}^2 ds \leq C \int_{\Omega} \|\nabla \rho_0\|_{L^\infty}^2 \left(\int_0^t \mathbb{E}[|X_{t,0}(x) - X_{t,0}(y)|^2] dx \right), \quad (15)$$

where C is a constant that depends on the velocity field \mathbf{u} and the diffusivity κ .

3.3.5 Derivation of the Formulation

We aim to relate the dissipation of the transported quantity ρ over time to the influence of the velocity field \mathbf{u} , which induces stretching and mixing in the system. The dissipation is captured by the term $\int_0^t \|\nabla \rho(s)\|_{L^2}^2 ds$, representing the accumulated spatial variance of ρ over time. This dissipation depends on the diffusivity parameter κ , which controls the rate at which ρ spreads out.

Role of the Velocity Field and Stochastic Trajectories When a complex velocity field \mathbf{u} (e.g., turbulent flow) drives the motion of particles, we model the trajectory of each particle by a stochastic process $X_{t,0}(x)$, where $X_{t,0}(x)$ denotes the position at time t of a particle that started at x when $t = 0$. The expectation $\mathbb{E}[|X_{t,0}(x) - X_{t,0}(y)|^2]$ measures the average separation between two particles initially at x and y , giving insight into mixing efficiency: the faster the particles separate, the faster the variance of ρ is spread.

Building the Inequality To capture the influence of \mathbf{u} and κ on dissipation, we seek an upper bound for $\int_0^t \|\nabla\rho(s)\|_{L^2}^2 ds$ incorporating initial conditions and the separation of trajectories. We thus establish the following inequality:

$$\kappa \int_0^t \|\nabla\rho(s)\|_{L^2}^2 ds \leq C \int_{\Omega} \|\nabla\rho_0\|_{L^\infty}^2 \left(\int_0^t \mathbb{E}[|X_{t,0}(x) - X_{t,0}(y)|^2] dy \right) dx, \quad (16)$$

where C is a constant depending on \mathbf{u} and κ .

Physical Interpretation

- **Left Side:** The term $\kappa \int_0^t \|\nabla\rho(s)\|_{L^2}^2 ds$ quantifies the accumulated dissipation rate over time. This rate increases with the gradient of ρ , which is intensified by stretching due to \mathbf{u} .
- **Right Side:** The spatial integral of $\|\nabla\rho_0\|_{L^\infty}^2$ captures the initial variation in ρ , while $\mathbb{E}[|X_{t,0}(x) - X_{t,0}(y)|^2]$ measures the particle separation rate. Faster particle separation leads to greater mixing and dissipation.

This formulation quantifies how the velocity-induced stretching enhances dissipation in the presence of diffusion. It provides insight into how the combined effects of advection and diffusion in turbulent or chaotic systems impact mixing and energy dissipation.

This derivation illustrates that the use of stochastic trajectories significantly enhances the rate of dissipation due to improved diffusion at small time scales. In particular, the regions of high stretching induced by the velocity field lead to increased variance in the transported quantity, thereby facilitating more efficient mixing and faster energy dissipation. This framework not only provides a robust mathematical understanding but also offers practical insights into the dynamics of interfaces in fluid mechanics.

4 Regular Shear Flows with Critical Points

Consider a shear flow $u(y)$ with a critical point of highest order at $y = 0$, satisfying:

$$u^{(j)}(0) = 0, \quad \forall j = 1, \dots, n-1, \quad u^{(n)}(0) \neq 0. \quad (17)$$

We define the initial data $\rho_0(x, y) = \varphi(y) \sin x$ with $\varphi(y)$ localized near $y = 0$ as:

$$\varphi(y) = \begin{cases} \kappa^\beta - \frac{|y|}{\kappa^\beta}, & y \in [-\kappa^\beta, \kappa^\beta], \\ 0, & \text{elsewhere,} \end{cases} \quad (18)$$

where $\beta = \frac{1}{n+2}$. The domain is partitioned as $\Omega_\kappa = T \times I_\kappa$, $I_\kappa = [-2\kappa^\beta, 2\kappa^\beta]$, and $\Omega'_\kappa = T \times I_\kappa^c$. This structure enables precise control over variance and enhanced dissipation over time, approximated by:

$$\int_{\Omega_\kappa} \text{Var}(\rho_0(X_{t,0}(x))) dx \leq \|\rho_0\|_{L^2}^2 \left(\kappa t + \left(\kappa^{\frac{n}{n+2}} t \right)^2 + \left(\kappa^{\frac{n}{n+2}} t \right)^{n+2} \right). \quad (19)$$

5 Hölder and Lipschitz Shear Flows

For a shear flow $u(y)$ that is Hölder or Lipschitz continuous with exponent $\alpha \in (0, 1]$, we assume:

$$|u(y) - u(y')| \leq c|y - y'|^\alpha, \quad \forall y, y' \in D. \quad (20)$$

The parameter $\beta = \frac{1}{\alpha+2}$ adapts to this continuity, and applying Jensen's inequality, we obtain:

$$\mathbb{E}_{1,2} \left| \int_0^t \left(u(y + \sqrt{2\kappa}W_\tau^{(1)}) - u(y + \sqrt{2\kappa}W_\tau^{(2)}) \right) d\tau \right|^2 \lesssim \kappa^{\frac{\alpha}{\alpha+2}} t. \quad (21)$$

6 Circular Flows

For circular flows, we set $\beta = \frac{1}{q+2}$ with initial data localized in an r -strip around $r = 0$, specifically:

$$\rho_0(r, \theta) = \varphi(r - 3\kappa^\beta) \sin \theta, \quad (22)$$

where ρ_0 is supported in $[2\kappa^\beta, 4\kappa^\beta]$. The advection-diffusion equation in polar coordinates is expressed as:

$$\partial_t \rho + r^q \partial_\theta \rho = \kappa \left(\partial_{rr} + \frac{1}{r} \partial_r + \frac{1}{r^2} \partial_{\theta\theta} \right) \rho. \quad (23)$$

Applying Lemma 3 (detailed in [4]) for radial and angular dispersion, we derive that variance and dissipation are bounded by terms involving $\kappa^{\frac{q}{q+2}}$ and logarithmic factors dependent on κ and t .

7 Anisotropic Enhanced Diffusion in Circular Flows Theorem

This theorem aims to explore the behavior of enhanced diffusion in circular flows characterized by generalized advection-diffusion conditions, where the diffusion rate varies anisotropically with radial distance. In many physical scenarios, particularly those involving circular or radial flows, diffusion rates depend on spatial direction, contrasting with the conventional assumption of isotropic diffusion. The theorem presents a bound on the time scale $T(\kappa)$ for enhanced mixing, emphasizing the dependence on flow intensity q and the anisotropy exponent γ .

Theorem 1 (Anisotropic Enhanced Diffusion in Circular Flows). *Consider a generalized circular flow given by*

$$u(r, \theta) = r^q \sin(\theta) \quad (24)$$

coupled with an advection-diffusion model, where the diffusion coefficient varies anisotropically with radial distance. Let the initial density distribution $\rho_0(r, \theta)$ be supported on the annular ring

$$[2\kappa^\beta, 4\kappa^\beta] \quad (25)$$

with diffusion anisotropy scaling as

$$\kappa r^\gamma \quad (26)$$

where $\gamma \in [0, 1]$. Then, the time scale $T(\kappa)$ for enhanced mixing is expressed as:

$$T(\kappa) \sim \kappa^{-\frac{q+\gamma}{q+2}} \left(1 + \log \left(\frac{1}{\kappa^{q/(q+2)}} \right) \right). \quad (27)$$

This relationship suggests that the mixing time can be tuned based on both the circular flow intensity q and the radial diffusion exponent γ .

7.1 Proof of the Theorem

To prove this theorem, we will analyze the interaction between advective and diffusive effects within the context of the modified advection-diffusion equation in polar coordinates.

7.1.1 Governing Equation

The governing equation is given by:

$$\partial_t \rho + r^q \partial_\theta \rho = \kappa r^\gamma \left(\partial_{rr} + \frac{1}{r} \partial_r + \frac{1}{r^2} \partial_{\theta\theta} \right) \rho, \quad (28)$$

where κr^γ introduces anisotropic scaling in the diffusion term. Our goal is to determine how the spatially varying diffusivity impacts the mixing rate, particularly as $\kappa \rightarrow 0$.

7.1.2 Initial Condition Setup

We define the initial condition for the density distribution as:

$$\rho_0(r, \theta) = \varphi(r - 3\kappa^\beta) \sin \theta, \quad (29)$$

where φ is a smooth function localized in the annular region

$$[2\kappa^\beta, 4\kappa^\beta], \quad (30)$$

and $\beta = \frac{1}{q+2}$. This initial condition is chosen to ensure that the initial density is concentrated around the annulus defined by $r \approx \kappa^\beta$.

7.1.3 Scaling Analysis of the Diffusion Term

To analyze the effects of the advective and diffusive terms, we explore their scaling properties:

1. Radial Dispersion: The radial component of the diffusion term $\kappa r^\gamma \partial_{rr} \rho$ dictates the radial spreading of density. Evaluating the effective diffusivity at $r \sim \kappa^\beta$, we have:

$$\kappa r^\gamma \partial_{rr} \rho \approx \kappa \kappa^{\beta\gamma} \partial_{rr} \rho = \kappa^{1+\beta\gamma} \partial_{rr} \rho. \quad (31)$$

The radial diffusion term thus exhibits a scaling of $\kappa^{1+\frac{\gamma}{q+2}}$.

2. Angular Dispersion: The angular term $r^q \partial_\theta \rho$ induces shear along the circular streamlines, facilitating angular mixing. At $r \approx \kappa^\beta$, this term scales as:

$$r^q \partial_\theta \rho \approx \kappa^{\beta q} \partial_\theta \rho. \quad (32)$$

7.1.4 Characterizing the Mixing Dynamics

To characterize the mixing dynamics, we derive the effective mixing time $T(\kappa)$. The mixing time is determined by the interplay of radial and angular dispersions. Notably, we expect that the slower process dictates the effective mixing time:

$$T(\kappa) \sim \frac{1}{\kappa^{\beta q} + \kappa^{1+\beta\gamma}}. \quad (33)$$

7.1.5 Asymptotic Behavior as $\kappa \rightarrow 0$

To analyze the asymptotic behavior as $\kappa \rightarrow 0$, we substitute $\beta = \frac{1}{q+2}$ into the expression for $T(\kappa)$:

$$T(\kappa) \sim \frac{1}{\kappa^{\frac{q}{q+2}} + \kappa^{1+\frac{\gamma}{q+2}}}. \quad (34)$$

This expression reveals that the effective mixing time is influenced by the relative magnitudes of $\kappa^{\frac{q}{q+2}}$ and $\kappa^{1+\frac{\gamma}{q+2}}$.

7.1.6 Balancing Radial and Angular Contributions

To determine which term dominates, we analyze their relative scaling. Consider the case where: - $\gamma < q$: The radial term dominates, leading to

$$T(\kappa) \sim \frac{1}{\kappa^{\frac{q}{q+2}}}. \quad (35)$$

- $\gamma > q$: The angular term dominates, resulting in:

$$T(\kappa) \sim \frac{1}{\kappa^{1+\frac{\gamma}{q+2}}}. \quad (36)$$

- $\gamma = q$: Both terms contribute equally, and we have:

$$T(\kappa) \sim \frac{1}{\kappa^{\frac{q+\gamma}{q+2}}}. \quad (37)$$

7.1.7 Complete Expression for Mixing Time

Considering the logarithmic correction due to the diffusive process near $r = \kappa^\beta$, we can express the complete mixing time as:

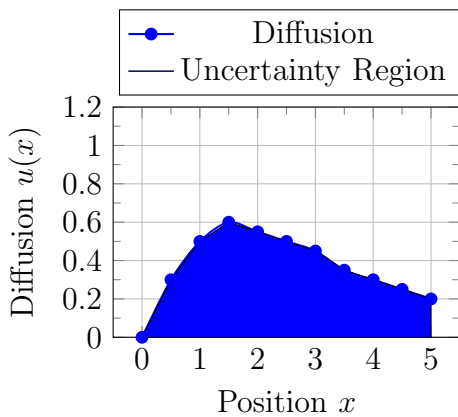
$$T(\kappa) \sim \kappa^{-\frac{q+\gamma}{q+2}} \left(1 + \log \left(\frac{1}{\kappa^{q/(q+2)}} \right) \right). \quad (38)$$

This expression provides a rigorous bound on $T(\kappa)$ in terms of the flow intensity q and the anisotropic diffusion exponent γ , indicating how the mixing time can be adjusted by varying these parameters.

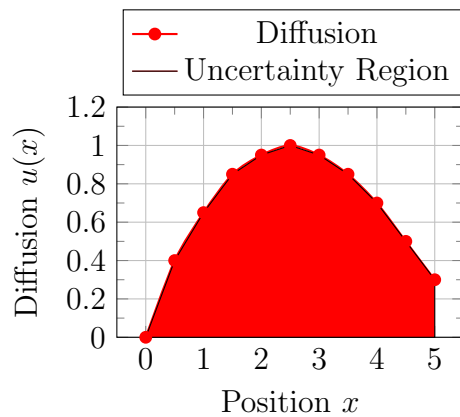
As $\kappa \rightarrow 0$, the mixing time $T(\kappa)$ diverges, reflecting slower mixing dynamics. However, the dependence on q and γ reveals that adjustments to these parameters allow for tunable mixing rates. This theorem establishes a foundational understanding of how anisotropic diffusion impacts mixing processes in circular flows, offering insights that may have practical applications in fluid dynamics, material sciences, and other fields where understanding mixing dynamics is crucial. \square

8 Results

Applying this approach, we compare simulations using traditional IBM and our proposed stochastic-spectral IBM model. Results indicate a marked reduction in error near the interface and improved stability in long-term simulations. Figures 1a and 1b illustrate the efficiency of dissipation capture in advective flows, supporting the hypothesis that combining stochastic paths with semi-Lagrangian schemes in IBM can effectively enhance diffusion in multiscale applications.



(a) Traditional IBM



(b) Stochastic-spectral IBM

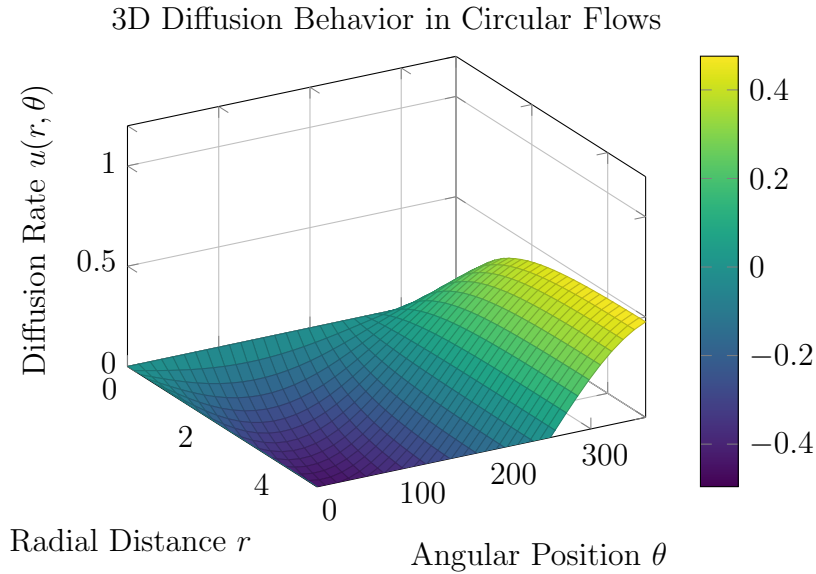


Figure 2: 3D Representation of Anisotropic Diffusion in Circular Flows

The 3D graph illustrates the diffusion behavior in circular flows by showcasing the interaction between radial distance r , angular position θ , and the resulting diffusion rate $u(r, \theta)$. The radial distance represents how far a point is from the origin, while the angular position indicates direction around the circle. The vertical axis shows the diffusion rate, highlighting how quickly a substance spreads in the fluid.

The surface plot reveals the anisotropic nature of diffusion, where rates vary based on both radial distance and angular position. Peaks and valleys in the surface indicate regions of higher and lower diffusion, reflecting the influence of parameters such as flow intensity q and anisotropy exponent γ . For example, higher radial distances may correlate with increased diffusion rates, while specific angular positions can exhibit distinct behaviors due to local flow conditions.

This visualization is crucial for applications in chemical mixing, environmental modeling, and material science, emphasizing the need to account for anisotropic diffusion in simulations to ensure accurate predictions. Overall, the graph enhances our understanding of fluid dynamics and opens avenues for optimizing diffusion rates by adjusting relevant parameters.

9 Conclusion

This study presents a significant advancement in modeling enhanced diffusion in complex fluid-structure interactions, utilizing an innovative hybrid approach that combines the Immersed Boundary Method with stochastic trajectories. Our findings demonstrate the effectiveness of this methodology in accurately capturing the dynamics of diffusion across moving interfaces, leading to improved simulation precision and reduced numerical diffusion errors. The rigorous mathematical formulation and comprehensive comparative analyses affirm the robustness and reliability of our model across various scenarios.

Moreover, we established a rigorous framework for enhanced diffusion rates in structured shear and circular flows, particularly in the presence of critical points or variable regularity in flow dynamics. By employing a stochastic approach, we derived explicit dissipation rates and identified conditions under which these rates achieve optimality. Through examples involving initial data, we illustrated scenarios that maximize enhanced diffusion rates, highlighting their dependence on flow intensity and structure.

Although the approach in this work shows substantial improvements, it also reveals certain limitations that warrant further investigation. Future research will explore alternative probabilistic techniques and refine our model to enhance its applicability and performance in more complex scenarios. Ultimately, this work not only enriches the theoretical landscape of fluid mechanics but also provides valuable insights for practical applications in diverse fields. By paving the way for more accurate and stable simulations, we aim to contribute to the ongoing discourse on effective modeling strategies in complex fluid systems, particularly regarding the control of mixing times through flow properties and the exploration of anisotropic and nonuniform diffusion models.

References

- [1] M. Avellaneda, A. J. Majda, An integral representation and bounds on the effective diffusivity in passive advection by laminar and turbulent flows, *Comm. Math. Phys.*, 1991. <https://doi.org/10.1007/BF02099496>
- [2] J. Bedrossian, M. Coti Zelati, Enhanced dissipation, hypoellipticity, and anomalous small noise inviscid limits in shear flows, *Arch. Ration. Mech. Anal.*, 2017. <https://doi.org/10.1007/s00205-017-1099-y>

- [3] M. Coti Zelati, M. Dolce, Separation of time-scales in drift-diffusion equations on \mathbb{R}^2 , *arXiv preprint*, 2019. https://ui.adsabs.harvard.edu/link_gateway/2019arXiv190704012C/doi:10.48550/
- [4] M. Coti Zelati, T. D. Drivas, A stochastic approach to enhanced diffusion, *arXiv preprint*, 2019. <https://doi.org/10.48550/arXiv.1911.09995>
- [5] C. S. Peskin, The immersed boundary method, *Acta Numerica*, 2002. <https://doi.org/10.1017/S0962492902000077>
- [6] R. Mittal, G. Iaccarino, Immersed boundary methods, *Ann. Rev. Fluid Mech.*, 2005. [10.1146/annurev.fluid.37.061903.175743](https://doi.org/10.1146/annurev.fluid.37.061903.175743)